Nanoscale

PAPER

View Article Online
View Journal | View Issue

Cite this: *Nanoscale*, 2015, **7**, 1081

Electrically driven plasmon mediated energy transfer between ZnO microwires and Au nanoparticles

Bin Zhao,[a,b] Ming-Ming Jiang,[a] Dong-Xu Zhao,*[a] Yang Li,[a] Fei Wang[a] and De-Zhen Shen[a]

Electrically driven energy transfer between the surface defect states of ZnO quadrilateral microwires (MWs) and localized surface plasmon polaritons has been realized by means of introducing Au nanoparticles (NPs). An electroluminescence device with green emission using ZnO quadrilateral MWs, was fabricated. Once the Au NPs are sputtered on the surfaces of the ZnO MWs, the electroluminescence of the ZnO MWs will shift from green to red. Meanwhile, dual emissions were observed by means of sputtering Au NPs on a single ZnO MW periodically. Due to the Au NPs, electrically driven plasmon mediated energy transfer can achieve the modulation of amplifying, or quenching the surface defect emission. The relevant dynamic process of the surface plasmon mode mediated energy transfer was investigated. This new energy transfer method potentially offers an approach of modification and recombination of the surface defect state excitations of wide bandgap semiconductor materials.

Received 16th September 2014,
Accepted 11th November 2014

DOI: 10.1039/c4nr05369a

www.rsc.org/nanoscale

1 Introduction

The energy transfer process involving the excitation energy from excited donor semiconductor nano/microstructures being transferred to metal nanostructures is of critical importance for the emerging field of plasmon-enhanced metal photoluminescence and plays an important role in diverse phenomena across physics, chemistry, and biology.[1–8] Examples include the effective transfer of excitation energy from donor molecules to acceptor molecules on opposite sides of metal films supported by coupled surface plasmon polaritons (SPPs).[9,10] This variant of SPPs mediating radiative transfer should allow directional control over the flow of excitation energy with the use of suitably designed metallic nanostructures. Comparing with non-radiative energy transfer (such as Förster Energy Transfer), radiative energy transfer has sufficient distance range but poor efficiency and directionality. The surface plasmons of exquisitely designed and optimized metal nanostructures are powerful tools to enhance the efficiency of both radiative and non-radiative energy transfer.[11–15]

Excitation energy transfer from donor to acceptor can be simply divided into two broad categories: radiative transfer, and non-radiative transfer. In contrast with non-radiative transfer, radiative transfer is a simple emission and absorption process. Radiative recombination in gold, copper, and gold–copper alloys has been observed arising from transitions between electrons in the conduction band states below the Fermi level and holes in the d bands generated by optical excitation.[16–19] Metal photoluminescence (PL) originates from the radiative recombination of photoexcited core holes and conduction band electrons, and can be enhanced due to the surface plasmon local field effect.[20] In addition to producing strong localized electric fields, resonant plasmons in noble metal nanostructures are also responsible for the absorption of photons to create excited or hot electrons in the metal. Interestingly, the inverse process, namely, of generating photons from non-equilibrium electrons in metal nanostructures themselves, can be facilitated by resonant plasmons as well. Consequently, PL in gold nanoparticles has been ascribed to the radiative damping of particle plasmons generated by the recombination of sp band electrons and excited d band holes.[11,18]

In contrast with conventional light sources, light-emitting diodes on the basis of wide bandgap semiconductor materials, such as ZnO and GaN, are becoming alternatives for future general lighting applications owing to their high efficiency and reliability.[21,22] The broad visible emission observed in ZnO has been attributed variously to interstitial zinc ions (Zn_i), oxygen

---

[a] *State key Laboratory of Luminescence and Applications, Changchun Institute of Optics, Fine Mechanics and Physics, Chinese Academy of Sciences, No. 3888 Dongnanhu Road, Changchun, 130033, People's Republic of China*
[b] *University of the Chinese Academy of Sciences, Beijing, 100049, People's Republic of China. E-mail: zhaodx@ciomp.ac.cn*

vacancies (V_O), chemisorbed oxygen, divalent copper impurities, and zinc vacancies (V_{Zn}). Presently, V_O are thought to be the likely cause of the visible emission around 500 nm.[23–31] Nevertheless, reports on the electroluminescence (EL) of surface defects are very rare.[31,32] Plasmon-enhanced band emission of ZnO has been achieved by the deposition of metals such as Ag, Au, Al, and Pt on ZnO films, as a result of the resonant coupling between the surface plasmons of the metal and the band gap emission of ZnO.[8,32–37] The quenching of exciton emission in semiconducting micro/nanostructures by fluorophores has been studied extensively over the past decade.[5,38,39] Previous reports have focused overwhelmingly on energy transfer from the exciton state of the micro/nanostructures.[1,2,8] To date, there have been no systematic studies of energy transfer from charge carriers in the defect or trap states of micro/nanostructures to acceptors.[34,40,41] Such studies are important in that surface defect state recombination limits the overall radiative quantum yield of the semiconductor micro/nanostructures. In some cases, the defect emission may even dominate over exciton emission.

However, some doubts remain about the involvement of plasmons in the EL process on the basis of bandgap semiconductor nano/microstructures, and agreement on a mechanism for the EL process in nanostructures is lacking.[35,38–42] Electrically driven excitation energy transfer from donor to acceptor is a rarely researched field, which should be given further attention. In this paper, detailed experimental and theoretical studies of the energy transfer from the defect states of ZnO microwires to Au NPs are presented. The visible defect emission of bare ZnO microwires was studied under electrically driven conditions. By means of introducing Au NPs, Au dimer localized surface plasmon resonances around 600 nm were demonstrated. Meanwhile, surface defect luminescence was suppressed and the luminescence center then transferred from 500 nm to 600 nm, which originated from radiative recombination of photoexcited localized surface plasmon resonances. The energy transfer process involving the interaction between surface defect states and surface plasmons was taken into account. In addition, Au NPs were sputtered periodically on a single ZnO microwire and dual emission fluorescence around 500 nm and 600 nm can be observed simultaneously.

2 Experimental section

The ZnO microwires were synthesised *via* a traditional chemical vapour deposition method in a horizontal tube furnace at 1000 °C. Glass substrates were cut into pieces of 1 cm × 1 cm, and strictly ultrasonically cleaned in acetone, ethanol and deionized water separately, for 15 minutes each. Subsequently, a ZnO microwire was selected to put on the substrates. Two indium (In) particles were put on the two ends of the ZnO MW as the electrodes. After annealing for 2 minutes at 400 °C, the ZnO MW can be fixed on the substrate. Then, metal–semiconductor–metal (MSM) structure based EL devices were fabricated. The Au nanoparticles were deposited on the surfaces of the ZnO MWs by a radio-frequency magnetron sputtering technique at room temperature with a pressure of 5×10^{-2} Pa, then the localized surface plasmon (LSP) enhanced MSM structure EL devices were fabricated.

The morphology of the ZnO MWs and Au NPs was characterized by field-emission scanning electron microscopy (FESEM) (model: Hitachi S-4800). The current–voltage (*I*–*V*) characteristics of the devices were measured using a Keithley 2611 system. The PL measurements of the ZnO MWs were performed using a He–Cd laser line of excitation wavelength 325 nm, and a micro-Raman spectrometer in a backscattering geometry configuration, which was used to obtain the emission spectra (model: LABRAM-UV Jobin Yvon), can focus on an area of 10 μm diameter and adjust the depth of the lasing focus. The fluorescence measurements of the Au NPs were performed using a xenon lamp of excitation wavelength 500 nm in a Hitachi F7000 fluorescence spectrophotometer. The EL spectra of the device were obtained using a Hitachi F4500 spectrometer. The EL phenomena can be observed in an optical microscope. The absorption spectra were carried out using a Shimadzu UV-3101 PC spectrophotometer.

3 Results and discussion

A schematic diagram of the ZnO based metal–semiconductor–metal (MSM) device is shown in Fig. 1, in which the ZnO microwire is modified by means of introducing Au NPs on the outer surfaces, periodically. A typical SEM image of a ZnO MW is shown in Fig. 2(a). The diameter of the ZnO MWs is about 10–15 μm and the length is about 1–2 cm. The inset indicates that the ZnO MWs possess a quadrilateral cross-section. Fig. 2(b) shows the *I*–*V* characteristics of the MSM device together with the Au NP coated ZnO MW based device. The *I*–*V* curve presents a linear relationship, which indicates the formation of the Ohmic contacts of the ZnO MWs. After introducing the Au NPs, the *I*–*V* characteristics show no changes, indicating

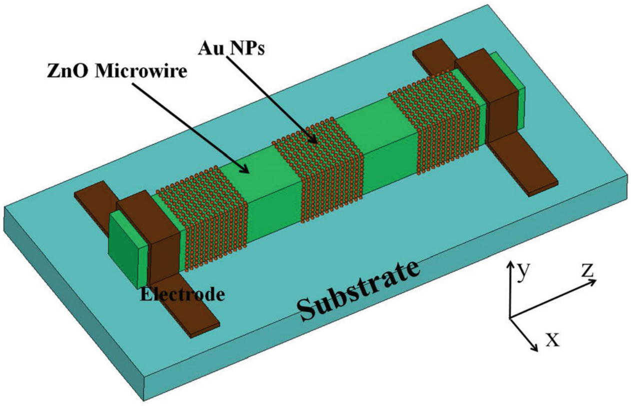

Fig. 1 Schematic diagram of the electrically driven electroluminescence device consisting of a ZnO microwire and Au NPs.

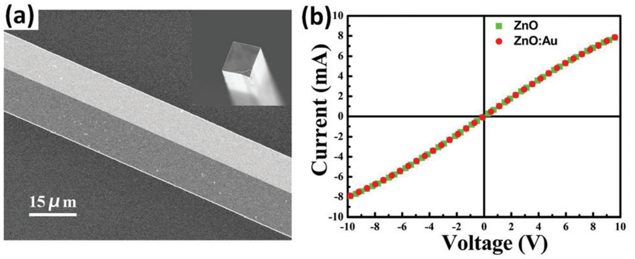

Fig. 2 Physical characteristics: (a) SEM image of a single ZnO microwire on a silicon substrate directed along the polar *c*-axis exhibiting a quadrilateral crystal symmetry, the inset shows the quadrilateral cross section; (b) the *I*–*V* characteristics of bare ZnO MW based EL devices, and Au NP coated ZnO MW based EL devices.

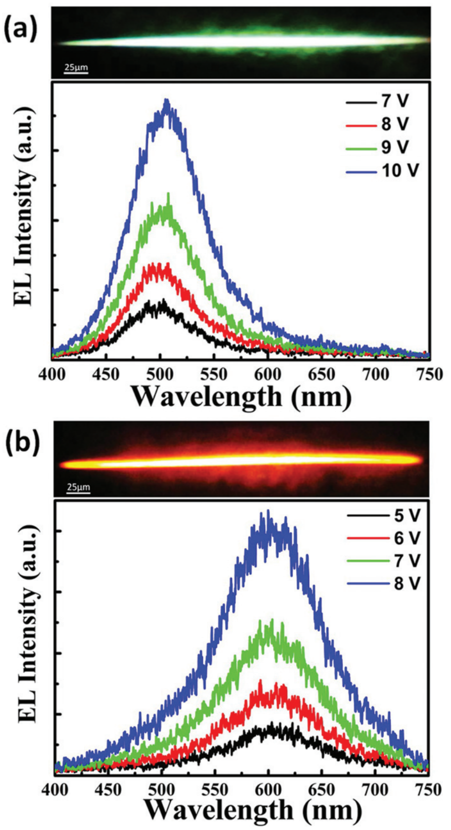

Fig. 3 Luminescence spectra under electrically driven conditions: (a) EL spectra of a bare ZnO MW operated from 7 V to 10 V, the inset is the camera image corresponding to the EL pattern (green) along the direction of the MW length; (b) EL spectra of a Au NP coated ZnO MW operated from 5 V to 8 V, the inset is the camera images corresponding to the EL pattern (red) along the direction of the MW length.

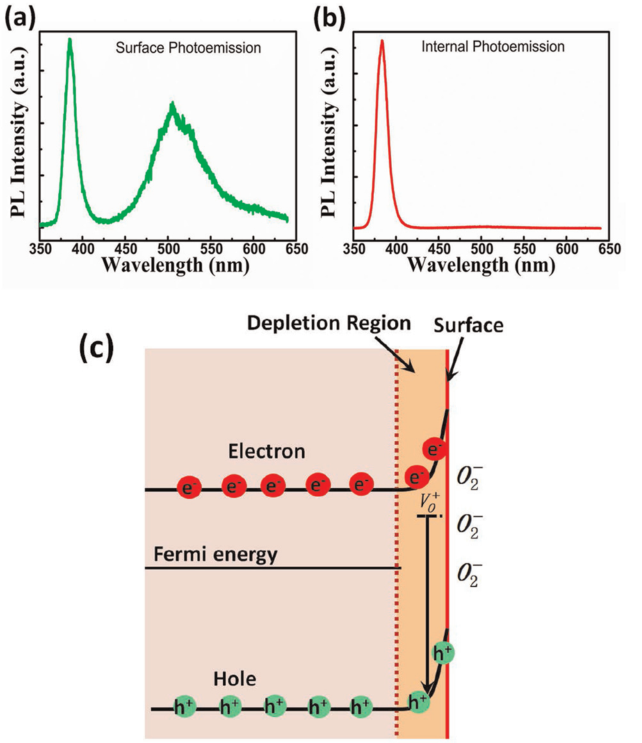

Fig. 4 Surface defect luminescence of bare ZnO MWs: (a) surface photoemission by means of keeping the pumping light focusing on the measured surface of the ZnO MW, which shows the surface defect luminescence center at around 500 nm; (b) internal photoemission by means of keeping the pumped light focused inside the measured ZnO MW, in which the defect luminescence can not be observed; (c) sketch of the energy band of the ZnO MW with the surface defect modes and the corresponding surface depletion region. The ZnO MWs possess high electron concentration, as well as a surface depletion region with small width, V_O^+ defect modes exist in the depletion region, the Fermi level is lower than the V_O^+ surface defect level, and almost all of the V_O^+ are filled.

that the Au NPs have no influence on the resistance of the ZnO MWs.

Fig. 3(a) illustrates the EL of a bare ZnO microwire, in which the spectra center is located at 500 nm under different injection currents. The inset shows a photograph of the green emission. Fig. 3(b) shows the EL of the ZnO microwire modified with Au nanoparticles, in which the luminescence center is located at around 600 nm under different injection currents. The inset shows a photograph of the red emission. Therefore, owing to the introduction of Au NPs, an obvious shift of the luminous center occurs from 500 nm to 600 nm. According to Fig. 3, it is obvious that the introduction of Au NPs can be used to modulate the luminescence center of ZnO MWs, meanwhile, suppression of the green emission can also be obtained. Previous studies have demonstrated that ZnO PL is sensitive to the presence of various adsorbates such as O_2, H_2, CO, and metal NPs;[23,27,28,43] however, few related reports on the EL mechanism, as well as the shift of luminescence centers on account of ZnO microwires, were demonstrated.[32,44]

In order to confirm the origin of the EL emission, PL measurements were performed. Fig. 4(a) demonstrates that there is a strong broad visible emission located at 500 nm, consistent with the EL spectra, which corresponds to the oxygen vacancy (V_O) defects of ZnO as described in previous reports.[23–28] Internal photoemission, by means of keeping the pumped light focusing inside the measured ZnO MW, as shown in the PL spectrum in Fig. 4(b), demonstrates that there is only an ultraviolet (UV) emission located at 387 nm, corresponding to the near-band-edge emission. Oxygen vacancies (V_O) are the most widely accepted mechanism for the visible emission of ZnO, and they can occur in three charge states: the doubly ionized oxygen vacancy (V_O^{++}) which does not capture any electrons and is doubly positively charged relative to the lattice of ZnO, the singly ionized oxygen vacancy (V_O^{+}) which has captured one electron and is singly positively charged relative to the lattice and the neutral oxygen vacancy (V_O^{x}).[23,24,27,43] According to the levels of these three oxygen vacancies in the energy band of ZnO, the origin of the green emitting peaks can be attributed to the electron transition from V_O^{+} centers to the valence band edge. In an atmospheric environment, oxygen molecules could be absorbed on the surfaces of ZnO MWs and then trap free electrons [$O_2 + e^- \rightarrow O_2{}^-$], thus creating a thin depletion layer near the surface.[45] A sketch of the energy band is shown in Fig. 4(c), which shows a depletion layer within the surface of the ZnO MWs. Free electrons are supplied by oxygen vacancies (V_O) [$V_O - e^- \rightarrow V_O^{+}$]. There are a large number of V_O^{+} defects existing within the surface depletion layers of the ZnO MWs, which have been confirmed by the PL measurements. A model based on the inelastic scattering of tunneling electrons has been proposed for the EL emission from the ZnO MW based MSM devices according to the previous report by our group.[46] The electrons under a high bias voltage have sufficient energy to scatter inelastically and then tunnel through the depletion layer to excite the defect states. In consequence, the green emission of EL is caused by the electron transition from V_O^{+} centers to the valence band edge near the surfaces of the ZnO MWs.

Taking the influence of the Au nanoparticles on the luminescence into account, the absorption spectra of the Au nanoparticles were recorded. Fig. 5(a)–(d) display the SEM images of the Au nanoparticle coated ZnO microwire. Fig. 5(a) displays the overall SEM image of the Au NP coated ZnO MW, the inset showing the corresponding bare ZnO MW. Therefore, the ZnO MWs have been coated by the Au NPs completely. Fig. 5(b)–(d) display the SEM images with different sputtering times; 30 s, 60 s, and 90 s. The absorption spectra displayed in Fig. 5(e) indicate that there is a strong absorption peak at around 600 nm. Therefore, the preparation of the random distribution of Au NPs could be used to excite dipole surface plasmon resonances at around 600 nm.[9,16,17,47,48] The shifts and intensities of the localized surface plasmon resonances can be derived from the densities of the Au NPs. The fluorescence spectra of the Au nanoparticles with different sputtering times are shown in Fig. 5(f), in which the luminescence center is located at around 600 nm with the help of an excitation source of 500 nm. Together with the absorption peak of the Au nanoparticles at around 600 nm as shown in Fig. 5(e), the absorption peak at around 600 nm can be responsible for the localized surface plasmon resonances of the Au NPs. This means that a Au NP plasmon mediated transfer process can be used to implement the amplification of EL at around 600 nm of the ZnO microwire. The detailed plasmon mediated transfer process will be described below.

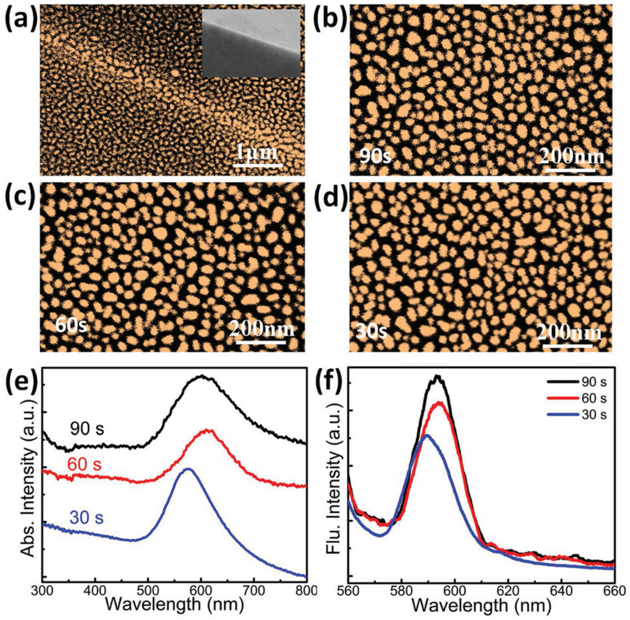

Fig. 5 (a) Displays the SEM image of the Au nanoparticle coated ZnO MW, the inset showing the corresponding bare ZnO microwire; (b)–(d) display the SEM images of the Au nanoparticles, with their corresponding sputtering times; (e) displays the corresponding absorption (Abs.) spectra; (f) displays the corresponding fluorescence (Flu.) spectra of the Au nanoparticles at an excitation of 500 nm.

According to the SEM images shown in Fig. 5(a)–(d), the diameter of the Au NPs is around D = 60 nm and a gap distance g ranging from 5 nm to 30 nm is obtained. Consequently, the extinction spectra of the Au NPs and the corresponding field distributions can be carried out by means of the time domain and frequency domain (FDTD) finite element methods.[49,50] In the calculation and simulation processes, the refractive index of the particles' environment was assumed to be $n_e = 1.7$, and the electromagnetic field was linearly polarized along a fixed interparticle axis. To approximate the experimental illumination conditions, the plasmon shift *versus* the interparticle separation relationship by averaging over a wide range of incident wave vectors and light polarizations, were taken into account. Fig. 6(a) shows the extinction spectra of a single Au NP with the diameter D ranging from 40 nm to 80 nm and the dipole surface plasmon resonances ranging from 420 nm to 530 nm, which gravely deviate from the experimental results. Therefore, the absorption peak shown in Fig. 5(e) cannot definitely be obtained from isolated Au nanoparticles. To account for these features of our experiments, Au NP dimer simulations were performed and are shown in Fig. 6(b). It indicates that surface plasmon resonances located at around 600 nm can be obtained. Therefore, dimers can be responsible for the absorption spectra of the Au NPs. Fig. 6(c) displays the electric field distributions of isolated and dimer Au NPs. Plasmon coupling in the dimers of metal NPs and the dependence on their distances could modulate the dipole surface plasmon resonances. Furthermore, plasmon

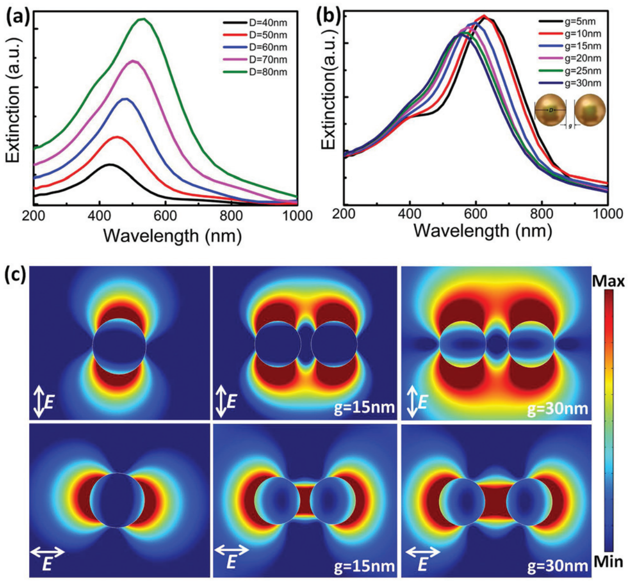

Fig. 6 Extinction spectra and field distribution of the Au NPs: (a) displays the extinction spectra of an isolated Au nanoparticle, with the diameter ranging from 40 nm to 80 nm; (b) displays the extinction spectra of a Au NP dimer, with a diameter D = 60 nm, and the gap distance g ranging from 5 nm to 30 nm; (c) displays the corresponding electric field distribution, with the parameter of D = 60 nm and the gap distances shown in the inset, the simulated resonance wavelength can be referred to the extinction spectra while the Au optical constants can be referred to ref. 49.

coupling would influence the absorption and release of energy by the gold nanoparticles.[14,17,19,51] Therefore, the size, shape and composition of the plasmonic nanostructures can be adapted to obtain a broad absorption.[6,11,18,52]

Radiative recombination in Au NPs has been observed, arising from transitions between electrons in conduction band states below the Fermi level and holes in the d bands generated by optical excitation.[17,19,20,53] The excitation process relies on the size of the nanoparticles, the materials that surround the particles, as well as the plasmon coupling induced by the distances between the nanoparticles.[19,50] This emission originates from the transition between the states near the Fermi energy, in contrast to the excited holes in the deep-lying bands. The luminescence derived from the radiative decay *via* re-emitted photons can be interpreted in terms of light scattering which involved surface roughness and which showed zero intensity for emission normal to the surface. The dependence of the peak emission wavelength on the Au NPs was consistent with the surface plasmon resonance. The luminescence was excited due to the EL from the ZnO MWs (500 nm). Following light absorption and local surface plasmon resonance excitation in these hybridized plasmonic structures, electromagnetic decay takes place radiatively through re-emitted photons as shown in Fig. 7(a). As we mentioned above, the Au NP dimer is responsible for the localized surface plasmon resonances at around 600 nm, therefore, localized surface plasmon resonance modes can be split into two kinds: the bright mode can be derived from electrically driven surface defect excitation, and the dark mode can be derived from the near field coupling interaction among Au NPs as shown in Fig. 6(c). The plasmon coupling among dimers guarantees that there is almost no wavelength shift. Simultaneously, the dark modes that appear cause the intraband transition of the NPs, and then induce the radiation loss, as shown in Fig. 7(b). Localized surface plasmon induced PL of Au NPs is generally considered to be a process in which electrons from the occupied d bands are first excited by a 520 nm pulsed laser, the absorption leads to unoccupied states of the sp conduction band. Then, subsequent intraband scattering processes prompt electron relaxation to the Fermi level. Eventually, the relaxation of the electron–hole pairs recombine either through non-radiative processes, or by means of the emission of luminescence. Radiative relaxation energies are therefore strongly connected to the interband separation. For the case of small particles where the optical properties are dominated by localized surface plasmon resonances, PL spectra can be observed, suggesting that the photoemission is related to the surface plasmons.[16,17,20,36,47,48]

The electronic energy will transfer from the MWs to the metal surface within a distance of less than 10 nm in a non-radiative process, and the efficiency is inversely proportional to the third power of the distance.[54] In the experimental procedure, the Au NPs were sputtered on the surfaces of the MWs, therefore, the Au NPs are in direct contact with the ZnO MWs. In the contact areas of the Au NP coated ZnO MWs, the radiative process would be suppressed, and then transitions will occur *via* the non-radiative process. Non-radiative decay in noble-metal nanostructures can take place through intraband excitations within the conduction band, or through interband excitations caused by transitions between other d bands and the conduction band (the corresponding radiation process can be referred to in Fig. 4). The d band energy levels lie 2.4 eV below the Fermi energy level for Au, making interband excitations considerably more unlikely than intraband excitations.[13,15,19,21,50] Fig. 7(b) depicts the parabolic conduction band of Au nanoparticles with a Fermi energy E_F. After non-radiative surface plasmon decay, electrons from occupied energy levels are excited above the Fermi energy. Localized surface plasmons in Au NPs can transfer energies between approximately 1 eV and 4 eV to hot electrons; this energy depends on the carrier concentration and the size and shapes of the nanostructures, shown in Fig. 7(c). After the injection of hot electrons, the plasmonic nanostructures are left positively charged because of electronic depletion. An electron-donor solution or a hole-transporting material is required to be in contact with the nanostructures, which can be used as carriers to transport the generated holes to the counter electrode, keeping the charge balance and sustaining an electric current. The further luminescence process is demonstrated in Fig. 7(d), that is, green emission can be produced due to the bare ZnO microwire, while red emission can be produced due to the Au nanoparticle coated ZnO microwire. The inset reveals the corresponding dual emitting phenomenon.[6,19,55]

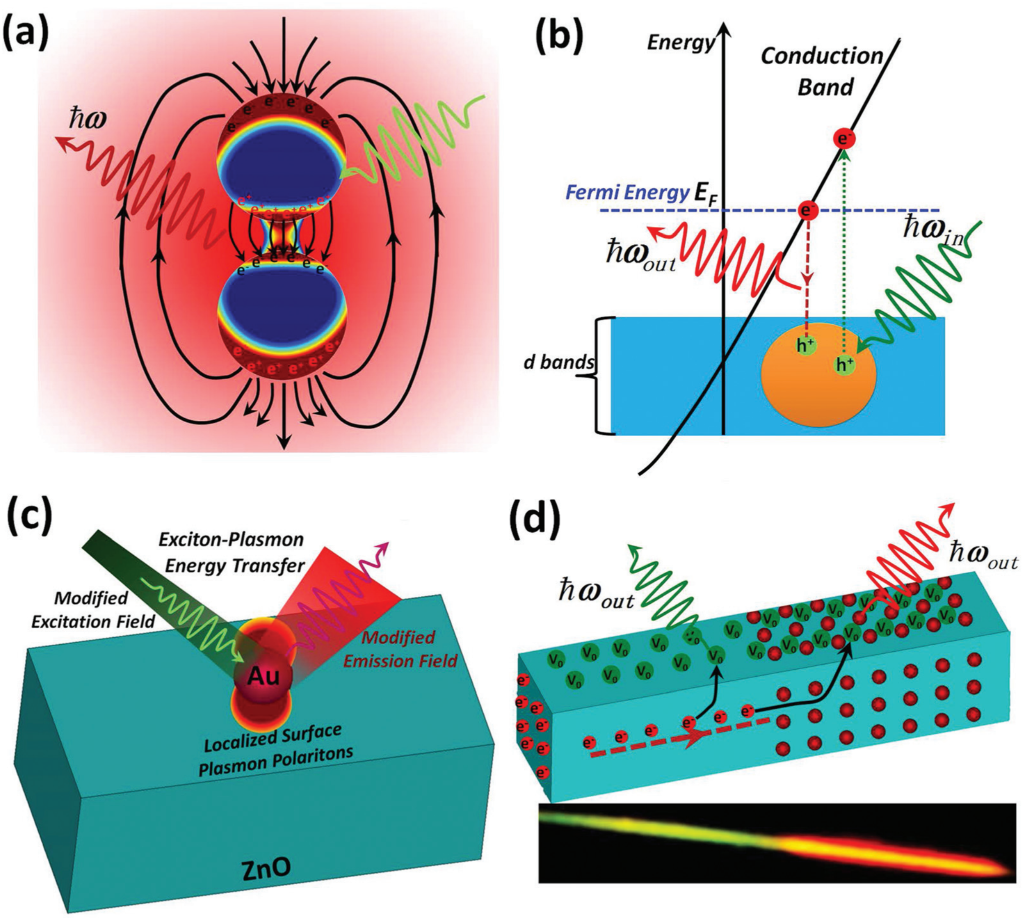

Fig. 7 Excitation and recombination mechanisms of the Au nanoparticles: (a) localized surface plasmons of Au dimers can decay radiatively *via* re-emitted photons; (b) schematic band structure of the Au nanoparticles showing the excitation and recombination transitions; (c) schematic of resonant exciton–plasmon interactions that can occur in metal–semiconductor hybridized plasmonic structures; (d) electrically driven induced electron transport process, which reveals surface defect mode excitation of the bare ZnO microwire, and the plasmon assisted enhancement and suppression mechanisms on the basis of the Au nanoparticle coated ZnO microwire.

To further demonstrate the excitation and recombination mechanisms, as shown in Fig. 7(d), the model was realized experimentally. Fig. 8 shows the dual emission process. Two independent luminescence centers located at around 500 nm and 600 nm, respectively, can be observed simultaneously. The corresponding emitting phenomenon observed using a camera in the microscope is shown in the inset of Fig. 8. The plasmon mediated energy transfer process is based on the concept that the Au NPs are treated as an excited acceptor, such as an oscillating dipole that can undergo energy exchange with a dipole resonant emission, which has a similar resonance frequency. Au NPs absorb the energy released from the surface defect emission at around 500 nm, providing a platform for the selective excitation of the localized surface plasmon resonances. Resonance energy transfer requires a spectral overlap between the donor emission and the acceptor absorbance spectra. In principle, if the surface plasmon resonance spectrum of the Au NPs overlaps the luminescence spectrum of an acceptor molecule, the donor can directly transfer its excitation energy to the acceptor *via* the exchange of a virtual photon. Therefore,

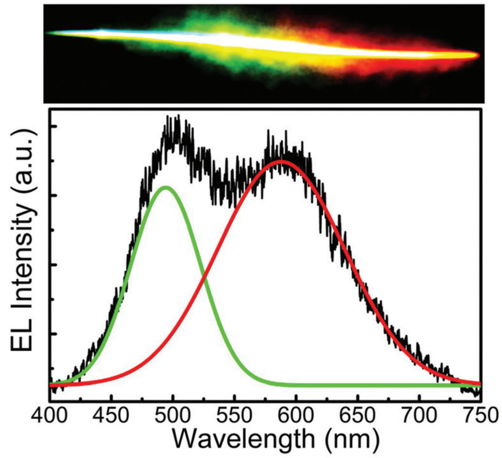

Fig. 8 Electroluminescence center fitting of surface defect modes based on the same ZnO microwire: the green line represents the surface defect luminescence of the bare ZnO microwire; the red line represents the plasmon mediated electroluminescence emitting process; the inset shows the camera image corresponding to the electroluminescence emitting along the microwire length direction.

the coupling interaction between metal plasmons and excitons occurs, which can achieve amplification of the emission. It is evident that there is no significant spectral overlap of the ZnO surface defect emission with the absorption spectra of the Au nanoparticles as shown in Fig. 4 and 5. In contrast, the overlap between the exciton emission of ZnO and the Au nanoparticle absorbance is negligible. The red emission center at around 600 nm can be attributed to energy released from the Au NP surface plasmon resonances.[20,37,43] In addition, metal photoluminescence originating from the radiative recombination of photoexcited core holes and conduction band electrons has been confirmed.[15,19,20] The Au nanoparticle surface plasmon local field effect can induce the enhancement of metal photoluminescence. Localized surface plasmons can decay radiatively *via* re-emitted photons, or non-radiatively *via* excitation of hot electrons. Therefore, both plasmon assisted enhancement and suppression mechanisms can be realized by means of the radiative recombination in Au nanoparticles arising from the transitions between electrons in conduction band states below the Fermi level and holes in the d bands generated by optical excitation. In order to confirm that the observed emission was not due to some other source such as Raman scattering from electrons, or another Au plasmon enhanced surface defect electroluminescence, Au nanoparticles were sputtered onto part of the ZnO microwire and it was found that red emission can be obtained from the region of the Au nanoparticle coated ZnO microwire as shown in Fig. 8. Meanwhile, the other metal NPs, such as Ag and Pt, were also explored, nevertheless, the luminescence processes cannot be observed.[10,53] The present results are quite unambiguous, and also no correction was taken into account for reabsorption in the present work.

The energy transfer process will be concentrated on in this section to display the plasmon-assisted enhancement and suppression mechanisms. The devices based on a single ZnO microwire partially coated with Au NPs by sputtering were built, as shown in Fig. 1. The EL and luminescent images shown in Fig. 8 display dual emission excitation. The detailed process can be referred to in Fig. 9. Fig. 9(a) shows the EL spectra at different injection currents. In the case of a small current injection, only the red emitting and the corresponding 600 nm luminescent centers can be observed. Once the incident current increases to a certain value, dual emission excitation can be achieved. Therefore, Au NP photoluminescence originating from the radiative recombination of photoexcited core holes and conduction band electrons is enhanced owing to the surface plasmon local field effect. Simultaneously, the inhibition and amplification phenomena induced by local surface plasmon resonance from 500 nm to 600 nm has been demonstrated explicitly. It can be found that the surface plasmons of Au NPs can not only enhance the radiative recombination of photoexcited core holes and conduction band electrons, but also maintain the energy release and transfer, and restrain the surface defect EL.[16,20,47,48] The investigation of detailed excitation and recombination mechanisms provides further evidence: firstly that Ohmic contact indicates that green emission is due to the surface defect modes, secondly that the introduction of Au nanoparticles can not only result in the ZnO defect state emission transfer, but also bring about the suppression, and thirdly that the quenching originates from a single process, which can be ascribed to energy transfer.[7,56]

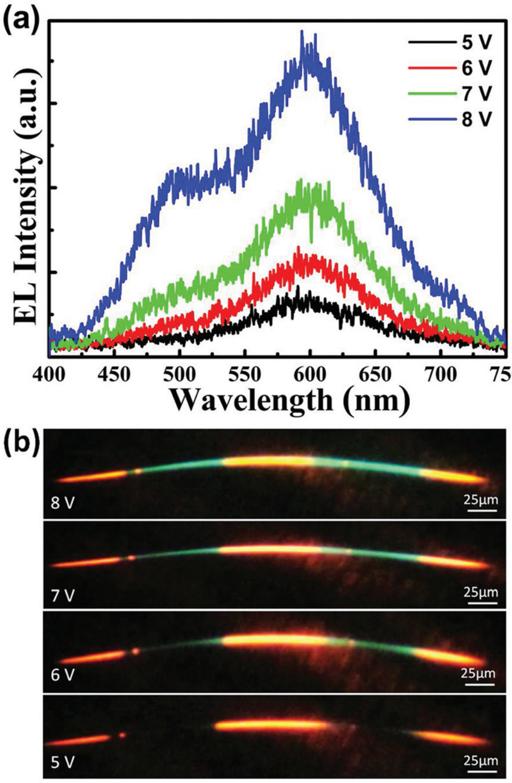

Fig. 9 Electroluminescence spectra based on the device shown in Fig. 1: (a) electroluminescence spectra operated between 5 V and 8 V; (b) the camera images corresponding to the electroluminescence pattern along the direction of the microwire length under different electrical injection currents.

4 Conclusion

Generally speaking, electrically driven plasmon mediated energy transfer between the surface defect modes of ZnO microwires and the localized surface plasmon modes of Au NPs has been realized. Electrically driven green emission has been obtained due to the V_O^+ defect states, which existed in the surface depletion region. By means of introducing Au nanoparticles, visible defect emission has been modified along with a red shift in the Au@ZnO microwires system. Intraband transition of the Au nanoparticles leads to radiative decay *via* re-emitted photons, which is responsible for the red emission. Excitation and recombination of the surface defect modes can be attributed to the Au NP dimers, which lead to signal suppression or amplification under electrically driven conditions. A direct application of the strategy outlined above would be to develop ZnO based light-emitting diodes. Another potential area of application is synthetic light harvesting and modulation structures; plasmonic modes could act to channel the energy transfer from absorbing species to reaction centers and more generally in photophysics near surfaces.

Acknowledgements

This work is supported by the National Basic Research Program of China (973 Program) under grant no. 2011CB302006 and 2011CB302004, the Key Program of the National Natural Science Foundation of China (11134009), the National Natural Science Foundation of China under grant no. 11404328 and 21101146, and the 100 Talents Program of the Chinese Academy of Sciences.

References

1 M. Lunz, X. Zhang, V. A. Gerard, Y. K. Gunko, V. Lesnyak, N. Gaponik, A. S. Susha, A. L. Rogach and A. L. Bradley, *J. Phys. Chem. C*, 2012, **116**, 26529–26534.

2 X. Zhang, C. A. Marocico, M. Lunz, V. A. Gerard, Y. K. Gunko, V. Lesnyak, N. Gaponik, A. S. Susha, A. L. Rogach and A. L. Bradley, *ACS Nano*, 2014, **8**, 1273–1283.

3 K. A. Velizhanin and T. V. Shahbazyan, *Phys. Rev. B: Condens. Matter*, 2012, **86**, 245432.

4 C. Zhang, M. L. F. Lerch, A. D. Martin, P. E. Simmonds and L. Eaves, *Phys. Rev. Lett.*, 1994, **72**, 3397–3400.

5 P. Andrew and W. L. Barnes, *Science*, 2000, **290**, 785–788.

6 V. N. Pustovit and T. V. Shahbazyan, *Phys. Rev. B: Condens. Matter*, 2011, **83**, 085427.

7 X. Zhang, C. A. Marocico, M. Lunz, V. A. Gerard, Y. K. Gunko, V. Lesnyak, N. Gaponik, A. S. Susha, A. L. Rogach and A. L. Bradley, *ACS Nano*, 2014, **8**, 1273–1283.

8 P. Andrew and W. L. Barnes, *Science*, 2004, **306**, 1002–1005.

9 M.-M. Jiang, H.-Y. Chen, C.-X. Shan and D.-Z. Shen, *Phys. Chem. Chem. Phys.*, 2014, **16**, 16233–16240.

10 B. P. Khanal, A. Pandey, L. Li, Q. Lin, W. K. Bae, H. Luo, V. I. Klimov and J. M. Pietryga, *ACS Nano*, 2012, **6**, 3832–3840.

11 V. Karanikolas, C. A. Marocico and A. L. Bradley, *Phys. Rev. A*, 2014, **89**, 063817.

12 R. Hildner, D. Brinks, J. B. Nieder, R. J. Cogdell and N. F. van Hulst, *Science*, 2013, **340**, 1448–1451.

13 C. Clavero, *Nat. Photonics.*, 2014, **8**, 95–103.

14 X. Fan, W. Zheng and D. J. Singh, *Light: Sci. Appl.*, 2014, **3**, e179.

15 M. Achermann, *J. Phys. Chem. Lett.*, 2010, **1**, 2837–2843.

16 H. Hu, H. Duan, J. K. Yang and Z. X. Shen, *ACS Nano*, 2012, **6**, 10147–10155.

17 E. Dulkeith, T. Niedereichholz, T. A. Klar, J. Feldmann, G. von Plessen, D. I. Gittins, K. S. Mayya and F. Caruso, *Phys. Rev. B: Condens. Matter*, 2004, **70**, 205424.

18 G. Schatz, *J. Phys. Chem. Lett.*, 2010, **1**, 2980–2981.

19 A. Mooradian, *Phys. Rev. Lett.*, 1969, **22**, 185–187.

20 T. V. Shahbazyan, *Nano Lett.*, 2013, **13**, 194–198.

21 Y.-Y. Lai, Y.-P. Lan and T.-C. Lu, *Light: Sci. Appl.*, 2013, **2**, e76.

22 E. Matioli, S. Brinkley, K. M. Kelchner, Y.-L. Hu, S. Nakamura, S. DenBaars, J. Speck and C. Weisbuch, *Light: Sci. Appl.*, 2012, **1**, e22.

23 C. Ton-That, L. Weston and M. R. Phillips, *Phys. Rev. B: Condens. Matter*, 2012, **86**, 115205.

24 A. Alkauskas, J. L. Lyons, D. Steiauf and C. G. Van de Walle, *Phys. Rev. Lett.*, 2012, **109**, 267401.

25 M. R. Wagner, G. Callsen, J. S. Reparaz, J.-H. Schulze, R. Kirste, M. Cobet, I. A. Ostapenko, S. Rodt, C. Nenstiel, M. Kaiser, A. Hoffmann, A. V. Rodina, M. R. Phillips, S. Lautenschläger, S. Eisermann and B. K. Meyer, *Phys. Rev. B: Condens. Matter*, 2011, **84**, 035313.

26 R. Vidya, P. Ravindran, H. Fjellvåg, B. G. Svensson, E. Monakhov, M. Ganchenkova and R. M. Nieminen, *Phys. Rev. B: Condens. Matter*, 2011, **83**, 045206.

27 A. Janotti and C. G. Van de Walle, *Phys. Rev. B: Condens. Matter*, 2007, **76**, 165202.

28 A. F. Kohan, G. Ceder, D. Morgan and C. G. Van de Walle, *Phys. Rev. B: Condens. Matter*, 2000, **61**, 15019–15027.

29 S. B. Zhang, S.-H. Wei and A. Zunger, *Phys. Rev. B: Condens. Matter*, 2001, **63**, 075205.

30 F. Stavale, L. Pascua, N. Nilius and H.-J. Freund, *J. Phys. Chem. C*, 2014, **118**, 13693–13696.

31 H. Y. Lin, C. L. Cheng, Y. Y. Chou, L. L. Huang, Y. F. Chen and K. T. Tsen, *Opt. Express*, 2006, **14**, 2372–2379.

32 S. T. Kochuveedu, J. H. Oh, Y. R. Do and D. H. Kim, *Chem. – Eur. J.*, 2012, **18**, 7467–7472.

33 C.-S. Wang, H.-Y. Lin, J.-M. Lin and Y.-F. Chen, *Appl. Phys. Express*, 2012, **5**, 062003.

34 Y.-M. Chang, M.-L. Lin, T.-Y. Lai, H.-Y. Lee, C.-M. Lin, Y.-C. S. Wu and J.-Y. Juang, *ACS Appl. Mater. Interfaces*, 2012, **4**, 6676–6682.

35 C. F. Guo, T. Sun, F. Cao, Q. Liu and Z. Ren, *Light: Sci. Appl.*, 2014, **3**, e161.

36 S. T. Kochuveedu and D. H. Kim, *Nanoscale*, 2014, **6**, 4966–4984.

37 M. Achermann, *J. Phys. Chem. Lett.*, 2010, **1**, 2837–2843.

38 H. Guo, Z. Lin, Z. Feng, L. Lin and J. Zhou, *J. Phys. Chem. C*, 2009, **113**, 12546–12550.

39 C.-H. Chen, S.-J. Chang, S.-P. Chang, M.-J. Li, I.-C. Chen, T.-J. Hsueh, A.-D. Hsu and C.-L. Hsu, *J. Phys. Chem. C*, 2010, **114**, 12422–12426.

40 A. J. Morfa, B. C. Gibson, M. Karg, T. J. Karle, A. D. Greentree, P. Mulvaney and S. Tomljenovic-Hanic, *Nano Lett.*, 2012, **12**, 949–954.

41 G. A. Beane, A. J. Morfa, A. M. Funston and P. Mulvaney, *J. Phys. Chem. C*, 2012, **116**, 3305–3310.

42 A. J. Morfa, N. Kirkwood, M. Karg, T. B. Singh and P. Mulvaney, *J. Phys. Chem. C*, 2011, **115**, 8312–8315.

43 Z.-M. Liao, H.-Z. Zhang, Y.-B. Zhou, J. Xu, J.-M. Zhang and D.-P. Yu, *Phys. Lett. A*, 2008, **372**, 4505–4509.

44 M.-M. Jiang, B. Zhao, H.-Y. Chen, D.-X. Zhao, C.-X. Shan and D.-Z. Shen, *Nanoscale*, 2014, **6**, 1354–1361.

45 C.-Y. Chen, J. R. D. Retamal, I.-W. Wu, D.-H. Lien, M.-W. Chen, Y. Ding, Y.-L. Chueh, C.-I. Wu and J.-H. He, *ACS Nano*, 2012, **6**, 9366–9372.

46 M. Ding, D. Zhao, B. Yao, B. Li, Z. Zhang, C. Shan and D. Shen, *J. Phys. D: Appl. Phys.*, 2011, **44**, 075104.

47 A. Bouhelier, R. Bachelot, G. Lerondel, S. Kostcheev, P. Royer and G. Wiederrecht, *Phys. Rev. Lett.*, 2005, **95**, 267405.

48 E. Dulkeith, T. Niedereichholz, T. Klar, J. Feldmann, G. Von Plessen, D. Gittins, K. Mayya and F. Caruso, *Phys. Rev. B: Condens. Matter*, 2004, **70**, 205424.

49 P. B. Johnson and R. W. Christy, *Phys. Rev. B: Solid State*, 1972, **6**, 4370–4379.

50 B. M. Reinhard, M. Siu, H. Agarwal, A. P. Alivisatos and J. Liphardt, *Nano Lett.*, 2005, **5**, 2246–2252.

51 N. J. Halas, S. Lal, W.-S. Chang, S. Link and P. Nordlander, *Chem. Rev.*, 2011, **111**, 3913–3961.

52 X. Wu, Y. Xiao, C. Meng, X. Zhang, S. Yu, Y. Wang, C. Yang, X. Guo, C.-Z. Ning and L. Tong, *Nano Lett.*, 2013, **13**, 5654–5659.

53 M. R. Beversluis, A. Bouhelier and L. Novotny, *Phys. Rev. B: Condens. Matter*, 2003, **68**, 115433.

54 A. Campion, A. Gallo, C. Harris, H. Robota and P. Whitmore, *Chem. Phys. Lett.*, 1980, **73**, 447–450.

55 J. Zheng, C. Zhou, M. Yu and J. Liu, *Nanoscale*, 2012, **4**, 4073–4083.

56 E. Khon, A. Mereshchenko, A. N. Tarnovsky, K. Acharya, A. Klinkova, N. N. Hewa-Kasakarage, I. Nemitz and M. Zamkov, *Nano Lett.*, 2011, **11**, 1792–1799.